AIAA JOURNAL
Vol. 43, No. 2, February 2005

Application of Simultaneous Perturbation Stochastic Approximation Method for Aerodynamic Shape Design Optimization

X. Q. Xing* and M. Damodaran†
Nanyang Technological University, Nanyang 639798, Republic of Singapore

Aerodynamic shape design optimization problems, such as inverse and constrained airfoil design and axisymmetric nozzle design, are investigated by applying the simultaneous perturbation stochastic approximation (SPSA) method to objective functions that are estimated during each design iteration using a finite volume computational fluid dynamics technique for solving the compressible Navier–Stokes equations. The SPSA method has been demonstrated in the literature as having significant advantages over stochastic global optimization methods such as the simulated annealing (SA) method. In this work the SPSA is compared with SA method for a class of two-dimensional and axisymmetric aerodynamic design optimization problems. The numerical studies show that the SPSA method is robust in reaching optimal aerodynamic shapes, is easy to implement, and is highly efficient. The SPSA method can also decrease the computational costs significantly compared with the SA method.

Introduction

AERODYNAMIC shape design problems are a typical class of complex design optimization problems that have been extensively investigated in recent years using computational fluid dynamics (CFD) as in Ref. 1. The characteristic features of such problems are the presence of a large number of design variables, complex constraints, and even discrete design parameter values. Unlike applications in structures and control systems, sensitivity information cannot be easily extracted from CFD codes. Hence, the characteristics of the entire flowfield must be computed to assess the objective function values during the aerodynamic shape design cycle. It is well known that the numerical computation of the flowfield characteristics is very time-consuming. In view of the enormous costs associated with evaluating the objective function, many optimization methods have been proposed in the literature to deal with these problems. Most of these methods fall into two categories; namely, deterministic methods and stochastic methods.

Deterministic optimization methods are efficient for finding the minima of continuously differentiable problems for which sufficiently accurate derivatives can be estimated at reasonable cost, but these methods do not always lead to a global optimum and often restrict the design space to conventional designs. Besides deterministic methods, stochastic methods such as genetic algorithms (GAs), simulated annealing (SA) algorithms, and so on have recently found applications in many practical engineering design optimization problems as well as nonengineering problems. Aly et al.[2] had applied SA to the design of an optimal aerodynamic shape of an axisymmetric forebody for minimum drag. GAs have also been successfully applied to aerodynamic shape optimization problems, such as airfoil shape design reported by Quagliarella and Cioppa[3] and Yamamoto and Inoue,[4] multi-element airfoil shape design reported by Cao and Blom,[5] and centrifugal compressor design reported by Benini and Tourlidakis.[6] These applications show that SA and GAs are all stochastic in nature and can easily be implemented in robust computer codes compared with deterministic methods. They also have the advantages of yielding a global minimum and in overcoming the limitations of deterministic gradient-based search methods, which have a tendency of having searches getting trapped in local minima. However, SA and GA methods require a large number of function evaluations and relatively long computation times, especially for the case of complex design problems. One approach to reduce computational time would be to use parallel GA and parallel SA. Gallego et al.[7] have shown that the parallel SA not only results in improved speedup but also increases the chances of searching for the global optima. Bhandarkar and Machaka[8] have discussed a variety of parallel schemes of SA. The division algorithm of Aarts and Korst[9] and the three parallelization strategies of Diekmann et al.[10] are also widely used. Wang and Damodaran[11,12] used parallel simulated annealing (PSA) to reduce the number of evaluations of the objective function for each processor and wall-clock time for a number of representative aerodynamic shape design optimization problems. Applications of parallel GA to improve the computational efficiency of aerodynamic design problems have also been reported by Vicini and Quagliarella[13] and Hämäläinen et al.[14] Although parallel SA and GA can speed up the computation, they still require enormous computational resources and effort. An attractive alternative to SA and GA that is investigated in this work is the simultaneous perturbation stochastic approximation (SPSA) method, which has been developed and described by Spall[15–17] and which has been applied to a number of difficult multivariate optimization problems. The SPSA method has attracted attention in many diverse areas such as statistical parameter estimation,[18] feedback control,[19–21] simulation-based optimization,[22] signal and image processing,[23,24] and so on. The essential feature of SPSA, which accounts for its power and relative ease of implementation, is the underlying gradient approximation, which requires only two measurements of the objective function to approximate the gradient regardless of the dimension of the optimization problem. It only uses objective function measurements and does not require direct measurements of the gradient of the objective function. This feature results in a significant decrease in the cost of optimization, especially in problems that have a large number of variables to be optimized. Based on its successful application in the wing design problem outlined by Xing and Damodaran,[25] the SPSA method is briefly outlined here and its performance as a viable optimization tool is demonstrated by applying it to aerodynamic objective functions obtained using CFD for inverse and constrained airfoil design, and axisymmetric nozzle design in this

Presented as Paper 2002-5643 at the AIAA/ISSMO 9th Symposium on Multidisciplinary Analysis and Optimisation, Atlanta, GA, 4–6 September 2002; received 24 March 2004; revision received 15 August 2004; accepted for publication 25 August 2004.

*Research Fellow, Singapore–MIT Alliance, School of Mechanical and Production Engineering, 50 Nanyang Avenue; xqxing@ntu.edu.sg.

†Associate Professor, Singapore–MIT Alliance Fellow, Division of Thermal Fluids Engineering, School of Mechanical and Production Engineering, 50 Nanyang Avenue; mdamodaran@ntu.edu.sg. Associate Fellow AIAA.

study. The performance of the SPSA method is also compared with that of the SA method.

Optimization Methods

Simultaneous Perturbation Stochastic Approximation Method

The problem of minimizing a scalar differentiable loss function $L(\boldsymbol{X})$, where $\boldsymbol{X}$ is a p-dimensional vector of design variables, can be treated as searching for the vector $\boldsymbol{X}^*$ such that $\partial L/\partial \boldsymbol{X} = 0$. This is the classical formulation of local optimization for differentiable loss functions and it is assumed that measurements of $L(\boldsymbol{X})$ are available for various values of $\boldsymbol{X}$. These measurements may or may not include added noise and no direct measurements of $\partial L/\partial \boldsymbol{X}$ are assumed available. The SPSA algorithm is usually defined in the general recursive SA form:

$$\boldsymbol{X}_{k+1} = \boldsymbol{X}_k - a_k g(\boldsymbol{X}_k) \tag{1}$$

where $g(\boldsymbol{X}_k)$ is the estimate of the gradient $\partial L/\partial \boldsymbol{X}$ at the iteration k based on the measurements of the loss function. Under appropriate conditions, the iteration in Eq. (1) will converge to $\boldsymbol{X}^*$ in some stochastic sense, as shown by Fabian[26] or Kushner and Yin.[27] The most essential part of this algorithm is the approximation of the gradient. If $y(\cdot)$ denotes a measurement of $L(\cdot)$ at a design level represented by the dot $(\cdot)$ then $y(\cdot) = L(\cdot) + \text{noise}$. One-sided gradient approximations involve measurements $y(\boldsymbol{X}_k)$ and $y(\boldsymbol{X}_k + \boldsymbol{\Delta X}_k)$, whereas two-sided gradient approximations involve measurements of $y(\boldsymbol{X}_k \pm \boldsymbol{\Delta X}_k)$. The simultaneous perturbation approximation has all the elements of the vector of design variables $\boldsymbol{X}_k$ randomly perturbed together to obtain two measurements of the objective function $Y(\boldsymbol{X}_k)$, but each component of $g(\boldsymbol{X}_k)$ is formed from a ratio involving the individual components in the perturbation vector and the difference in the two corresponding measurements. For a two-sided simultaneous perturbation, this approximation is given as

$$g(\boldsymbol{X}_k) = \frac{y(\boldsymbol{X}_k + c_k \boldsymbol{\Delta}_k) - y(\boldsymbol{X}_k - c_k \boldsymbol{\Delta}_k)}{2c_k} \begin{bmatrix} \Delta_{k1}^{-1} \\ \Delta_{k2}^{-1} \\ \vdots \\ \Delta_{kp}^{-1} \end{bmatrix} \tag{2}$$

for a vector of p design variables. The parameter $c_k = c_0/(k^m)$, where c_0 is a small positive number and m is a coefficient that is assigned a value of $\frac{1}{6}$ in this study. The term $\boldsymbol{\Delta}_k$ represents the random perturbation vector generated by Monte Carlo approaches and the components of this perturbation are independently generated from a zero-mean probability distribution. One simple distribution that has been used in this study is the Bernoulli ± 1 distribution with probability of $\frac{1}{2}$ for each ± 1 outcome. The implementation of the SPSA method requires only two measurements, which are independent of p because the numerator is the same for all the p design variables. This aspect enables the SPSA method to achieve significant savings in the total number of measurements required when p is large.

The SPSA algorithm starts by iterating from an initial guess of the optimal vector $\boldsymbol{X}_0$. First, the counter index k is initialized to a value of 0. Then an initial guess of the design variable vector $\boldsymbol{X}_k$ and nonnegative empirical coefficients are defined. Next a p-dimensional random simultaneous perturbation vector $\boldsymbol{\Delta}_k$ is constructed and two measurements of the objective function, namely $y(\boldsymbol{X}_k + c_k \boldsymbol{\Delta}_k)$ and $y(\boldsymbol{X}_k - c_k \boldsymbol{\Delta}_k)$, are obtained based on the simultaneous perturbation around the given vector $\boldsymbol{X}_k$. Then the simultaneous perturbation approximates to the gradient $g(\boldsymbol{X}_k)$ using Eq. (2). This is followed immediately by the updating of the design vector $\boldsymbol{X}_k$ to a new value $\boldsymbol{X}_{k+1}$ using the general recursive SA form, $\boldsymbol{X}_{k+1} = \boldsymbol{X}_k - a_k g(\boldsymbol{X}_k)$, where the parameter $a_k = a_0/(A+k)^\alpha$; a_0, A, and α can be chosen to ensure an effective practical performance of the algorithm. In this study, $a_0 = 0.167$ and $A = 300$ for the airfoil shape design problem, and $A = 1$ for the nozzle shape design problem; α is taken to be 1. Finally the algorithm is terminated if there are insignificant changes in several successive iterations or if the maximum allowable number of iterations has been reached. The details of the step-by-step implementation of the SPSA algorithm are explained by Spall.[15–17] The choice of the coefficients and parameters pertaining to the algorithm is crucial for the performance of the SPSA (as is the case with the choice of coefficients and parameters pertaining to all other stochastic optimization algorithms such as SA). Some useful guidelines for choosing the values of these coefficients and parameters can be found in Refs. 15–17, 26, 28, and 29.

Simulated Annealing Algorithm

The SA method resembles the cooling process of molten metals through annealing. At high temperatures, the atoms in the molten metal can move freely with respect to each another, but, as the temperature is reduced, the movement of the atoms gets restricted. The atoms start to get ordered and finally form crystals having the minimum possible energy. However, the formation of the crystals depends on the specified cooling rate. If the temperature is reduced at a very fast rate, the crystalline state may not be achieved at all; instead, the system may end up in a polycrystalline state, which may have a higher energy state than the crystalline state. Therefore, to achieve the absolute minimum energy state, the temperature needs to be reduced at a slow rate. The process of slow cooling is known as annealing in metallurgical parlance. Specific details of the SA algorithm and its implementation can be found in Ref. 30.

In this study, SA is based on Monte Carlo techniques and starts with a high temperature corresponding to the cycle $N = 1$. The objective function is calculated based on an initial (baseline) configuration (defined by the initial state of the vector of design variables) and this is followed by the random generation of a new configuration (new vectors of design variables). New trial points are generated around the current design vector by applying random moves along each design coordinate. The new design coordinate values are uniformly distributed in intervals around the corresponding coordinate and a step vector is used to guide the extent of the random moves. The step vector $\boldsymbol{V}_M$ is adjusted periodically through the step adjustment vector $\boldsymbol{H}$, N_T times to adapt to the behavior of the objective function. The new configuration is accepted as the current configuration if this change in the objective function is less than or equal to zero or if the change is greater than zero, provided the change in objective function also satisfies the Metropolis criterion, which measures the acceptance probability. The random generation of new design vectors and the satisfaction of the acceptance criteria are repeated N_s times until the Markov chain has completed at a given temperature. Then the temperature is lowered via temperature reduction factor R_T, a new sequence of moves is generated, and the cycle is repeated until the design vector converges to the optimum value. Tuning parameters are crucial for improving the performance of the optimization method. Details of the tuning parameters of SA have been outlined by Lee.[31] The values of the SA tuning parameters employed for this study are as follows: $R_T = 0.1$, $V_M = 0.001$, $H = 2.0$, $N_S = 10$, and $N_T = 5$ for the inverse airfoil design problem; $R_T = 0.1$, $V_M = 0.001$, $H = 1.0$, $N_S = 20$, and $N_T = 10$ for the transonic airfoil drag minimization problem; and $R_T = 0.25$, $V_M = 0.05$, $H = 2.0$, $N_S = 10$, and $N_T = 5$ for the two-dimensional axisymmetric nozzle design problem.

Application of Simultaneous Perturbation Stochastic Approximation in Aerodynamic Shape Design Problems

Inverse Airfoil Design Problem

Problems concerning the design of transonic airfoil shape to satisfy desired aerodynamic characteristics can be classified as constrained and unconstrained design optimization problems. An example of an unconstrained design problem is the inverse design problem of determining the airfoil shape that will support a target airfoil surface pressure distribution. This shape is determined by minimizing the discrepancy between the target and the evolving airfoil surface pressure distribution corresponding to the designed airfoil.

A baseline NACA 0012 airfoil is chosen and a steady flowfield around it at a Mach number of 0.73 and angle of attack of 2.78 deg is computed for starting the design cycle iterations. The airfoil shape is updated by adding smooth perturbations $\Delta y_k(x)$, defined as a linear combination of a family of smooth curves over the range $0 < x < 1$

as follows:

$$\Delta y_k(x) = \sum_{k=1}^{K} \delta_k f_k(x) \tag{3}$$

where x is the normalized chordwise position of the coordinates defining the airfoil contour, δ_k are the design variables which will change during the design iterations, K is the number of basis functions $f_k(x)$, and $K = 14$ for this study. Seven basis functions are used to define the upper surface while the remaining seven basis function define the lower surface. Hicks and Henne functions[32] are used as the basis functions to represent the airfoil shape and to restrict the design space in this study.

The leading edge and the trailing edge are fixed at the origin and a chord length away from the origin, respectively, along the x axis. For inverse design problems, a typical objective function to be minimized, $F(\boldsymbol{X})$, is defined as follows:

$$F(\boldsymbol{X}) = \left[\sum_{m=1}^{M} \left(Cp_{t_m} - Cp_{b_m} \right)^2 \Delta S_m \Bigg/ \sum_{m=1}^{M} \Delta S_m \right]^{\frac{1}{2}} \tag{4}$$

where Cp_{t_m} is the pressure distribution of the target airfoil, which for this example is a RAE 2822 airfoil at the same Mach number and angle of attack as that of the baseline airfoil; Cp_{b_m} is the pressure distribution of the designed airfoil which evolves with each design iteration; ΔS_m is the length of the airfoil surface element; and the summation is done for the M coordinate points defining the airfoil profile. Details of this process have been outlined by Lee and Damodaran.[33]

Transonic Airfoil Drag Minimization

The optimization of selected aerodynamic parameters such as aerodynamic lift, drag, or pitching moment subject to some imposed design constraints generally belongs to the class of constrained optimization problems. A typical constrained design problem is that of the transonic airfoil drag minimization, where the aim is to obtain an airfoil shape that produces minimum transonic drag at a specified flight condition while maintaining the lift at the original level. Two inequality constraints are imposed to ensure that the aerodynamic lift and cross-sectional area of the airfoil do not decrease during the optimization process. The constrained design problem is defined as follows:

Minimize

$$F(\boldsymbol{X}) = C_d \tag{5}$$

subject to

$$g_1(\boldsymbol{X}) = 1 - C_l/C_{l_0} \leq 0, \qquad g_2(\boldsymbol{X}) = 1 - A/A_0 \leq 0 \tag{6}$$

where $\boldsymbol{X}$ is the vector of k design variables δ_k; C_l and C_d are the aerodynamic lift and drag coefficients, respectively; A is the airfoil profile area; A_0 is the area of the baseline airfoil profile; and C_{l_0} denotes the initial value of the lift coefficient, which has to be maintained during the design optimization process. The baseline airfoil that is used to initiate this design optimization process is the RAE 2822 airfoil immersed in transonic flow at a Mach number of $M = 0.726$, angle of attack $\alpha = 2.44$ deg, and Reynolds number $Re = 6.5 \times 10^6$. The aerodynamic lift and drag values at this flight condition are first computed. The aim of optimization is to improve the aerodynamic shape of this baseline airfoil so that the drag can be minimized while maintaining the same lift and airfoil area. Here an external penalty function method is used to incorporate the constraints so that the composite function to be minimized can be defined as

$$F(\boldsymbol{X}) = C_d + \lambda_k \sum_{j=1}^{2} \{\max[0, g_j(x)]\}^2 \tag{7}$$

where $\lambda_{k+1} = 5\lambda_k$ when any $g_j(\boldsymbol{X}) > 0$.

Axisymmetric Nozzle Shape Design Optimization

This problem concerns the search for the optimal two-dimensional axisymmetric shape of the nozzle that maximizes the thrust of the nozzle. A two-dimensional CFD solver for solving Navier–Stokes equations is used to compute the internal flowfield from which the objective function is evaluated for each iterated aerodynamic shape. The objective function to be optimized is defined as

$$F(\boldsymbol{X}) = \frac{\rho_0 u_0^2}{P_0} \int P \, \mathrm{d}S \tag{8}$$

where $\mathrm{d}S = \pi(y_{i+1}^2 - y_i^2)$ is the elemental circular cross-sectional area of the nozzle; y_{i+1} and y_i are the radii at the grid points $i+1$ and i; ρ_0 and u_0 are the inflow density and velocity, respectively, which are used as reference values for scaling flow quantities in internal flow simulations using CFD analysis; P_0 is the inlet pressure; and $\boldsymbol{X}$ is the vector of design variables. Two design variables, namely inlet expansion half-angle and outlet expansion half-angle of the nozzle wall, are used for the shape optimization process in this study. Here the maximization of the objective function is done by the minimization of its reciprocal: $f(\boldsymbol{X}) = 1/F(\boldsymbol{X})$. The convergence plot shown for this case is based on $f(\boldsymbol{X})$. For this study, the constraints are specified in a simple way; that is, the design variables are only subject to the defined upper and lower bound limits. Both the SA method and the SPSA algorithm are used for the optimization, and the termination criterion for the convergence is set when the absolute change in the objective function between a certain number of user-defined consecutive design iterations is less than 10^{-3} or the maximum number of iterations has been reached.

Computational Fluid Dynamics Analysis for Evaluating Objective Functions

Numerical methods for solving the Navier–Stokes equations are used for computing the flowfield. The computation is updated in time from a set of initial conditions by a suitable time-marching algorithm. The flow analysis module used to evaluate the objective function is based on the finite volume formulation of the unsteady Navier–Stokes equations for two-dimensional viscous flow. For airfoil design problems (including inverse design problem and drag minimization problem), the equations are advanced from a set of initial conditions to steady-state solutions for the desired flow conditions by a multistage time-stepping scheme. Several convergence acceleration strategies, such as local time-stepping, implicit residual smoothing, and multigrid strategies, are used to accelerate the computation of steady-state solutions. Characteristic boundary conditions are imposed at the far-field boundaries, and a no-slip condition is imposed on the airfoil surface, which is also assumed to be adiabatic. A simple algebraic turbulence model is used to address the turbulence closure. The readers can refer to Jameson et al.[34,35] and Damodaran and Lee[36] for specific details of the flow modeling. A structured C grid of 128×48 cells is used for the CFD analysis. The objective function to be minimized is estimated for each design iteration by the CFD solver solving the unsteady compressible Navier–Stokes equations. The objective function is then minimized using the SPSA method. For the two-dimensional nozzle shape design problem, these equations are solved by the lower–upper symmetric Gauss–Seidel implicit scheme proposed by Yoon and Jameson,[37] and for enhancing the convergence and improving resolution, the scheme is extended using the total variation diminishing (TVD) scheme of Yee and Harten.[38] The code has been verified for a number of benchmark test problems by Wang et al.,[39] and a simple algebraic turbulence model is used in the present study for viscous flows. A structured grid of 41×101 grids with grids clustered near the nozzle wall surface is used for the CFD analysis. The inlet Mach number of the nozzle is 4.84 and the Reynolds number based on the diameter of inlet is $Re = 1.35E + 8$. The values of the radii are 0.5 m at the inlet section and 1.0 m at the exit. The length of the nozzle is 2.52 m.

Results and Discussion

Airfoil Inverse Design Problem

Computed results pertaining to the inverse airfoil shape design optimization problem using SPSA and SA methods are compared

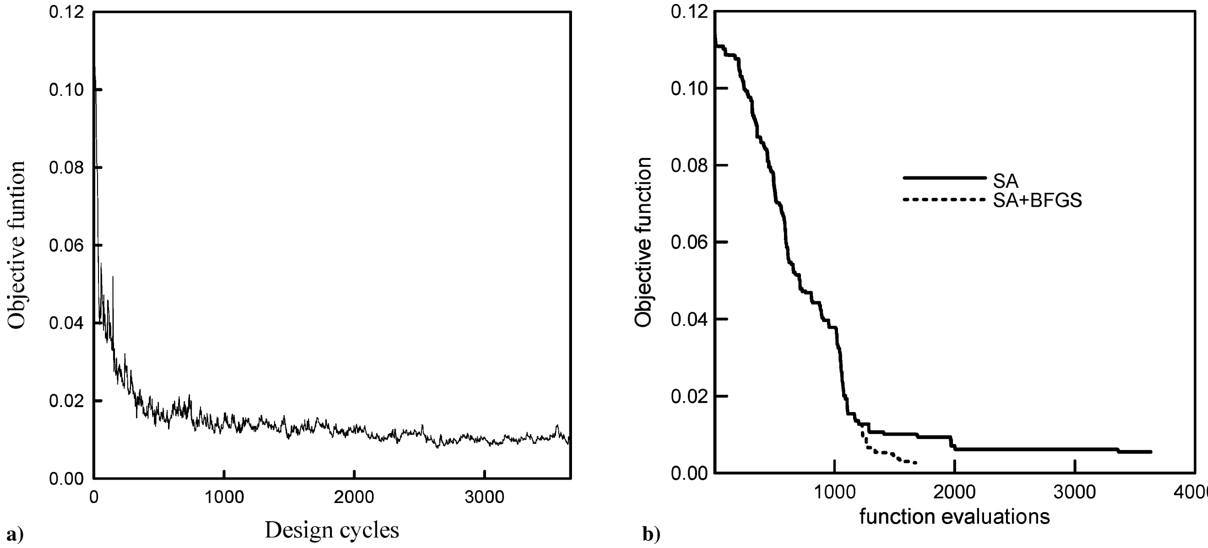

Fig. 1 Convergence history of the inverse design problem: a) SPSA method and b) SA method and hybrid SA.

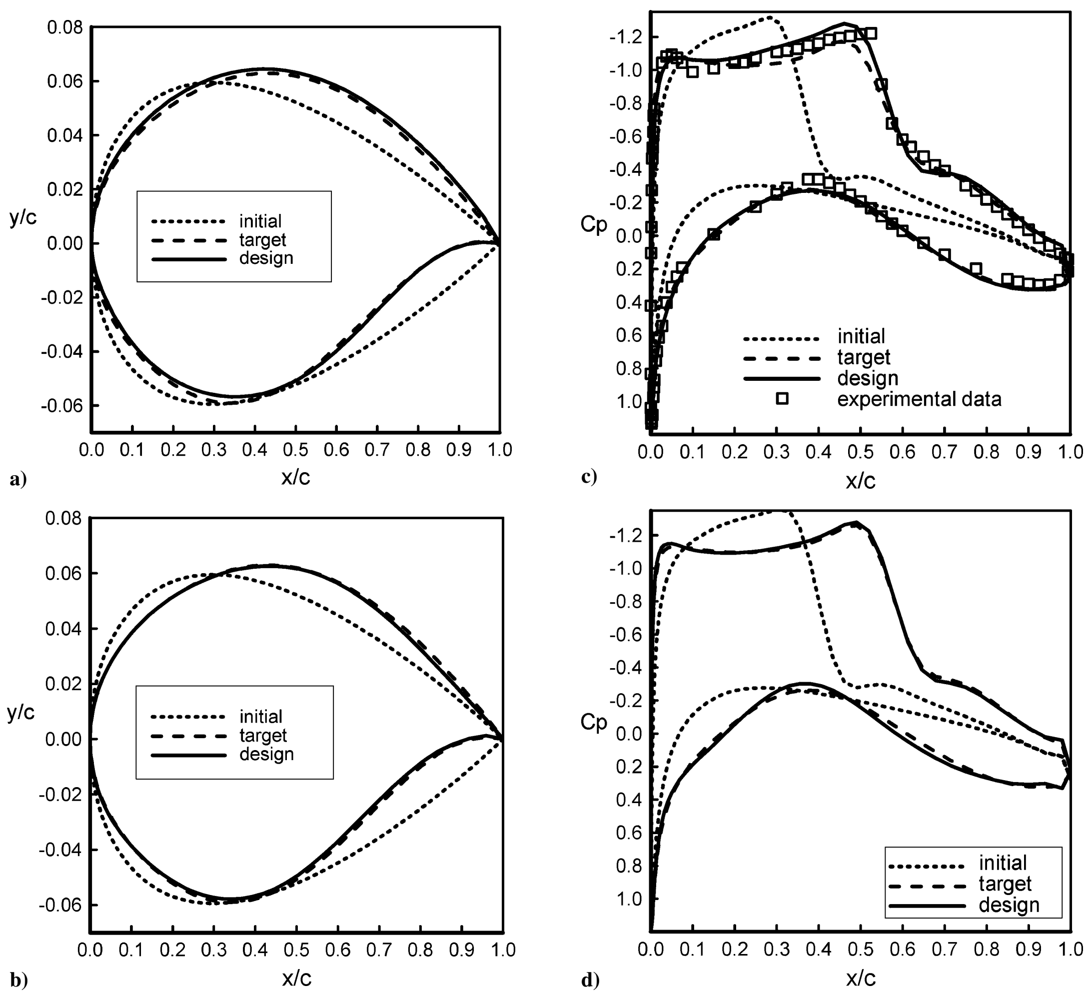

Fig. 2 Initial, design, and target airfoil shapes: a) SPSA method, b) SA method and surface pressure coefficient distributions, c) SPSA method, and d) SA method.

in Figs. 1 and 2. Figure 1 compares the convergence of the minimization of the objective function with design cycles. Comparison of Figs. 1a and 1b shows that the SPSA method requires fewer function evaluations to reach the target design than that required using SA. SPSA requires about 800 iterations (i.e., 2400 objective function evaluations to reach convergence) whereas the SA method requires about 2000 accepted function evaluations or about 4000 objective function evaluations because only about half of the objective function evaluations are accepted using the SA method. This suggests that the SPSA method provides a reasonable computational advantage over the SA method, which results from the fact that the SPSA method requires only two measurements of the objective function to approximate the gradient regardless of the dimensions of the design space corresponding to the optimization problem and consequently the cost of optimization decreases.

Figures 2a and 2b compare the initial, target, and designed airfoil shapes while Figs. 2c and 2d compare the corresponding airfoil surface pressure distributions computed using SPSA and SA methods, respectively. In Fig. 2c, the computed surface pressure distribution is also compared with the experimental data from Cook et al.[40] (case 6) for the RAE 2822 airfoil at Mach number 0.73, angle of attack $\alpha = 2.78$ deg, and $Re = 6.5 \times 10^6$. The good agreement between the computed and experimental data suggests that the numerical simulation is reasonably accurate. It can be seen from Fig. 2 that the discrepancies of the pressure distribution between the target and the designed airfoil obtained by the SPSA method are larger than that obtained by the SA method. This is also verified by the discrepancies of the airfoil shapes between the target and the designed airfoils. However, as mentioned earlier, the computational cost of the SPSA method is only half that of the SA method. The possibility of combining the SPSA method with other optimization methods to exploit the high rate of reduction of the objective function at the inception of the design process using SPSA to drive the design toward the optimal design zone first, followed by the use of other methods to perform the final stages of the convergence toward the optimal solutions to improve the design accuracy or to decrease the discrepancies of the pressure distribution between the target and the designed airfoil further, has also been explored. Here SPSA has been combined with SA and the gradient-based Broydon–Fletcher–Goldberg–Shanno (BFGS)[41] method, respectively. The hybrid SPSA with the BFGS method has also been explored by Xing and Damodaran[42] to see whether hybrid optimization methods could improve the design accuracy and cut the computational cost.

Prior to combining the SPSA method or the SA method with other optimization methods, the convergence histories are first examined to determine the switchover point for changing the optimization scheme. It can be observed from Fig. 1a that SPSA reduces the objective function value rapidly to about 0.012 in 800 design cycles, and after that the rate of reduction appears to be flat. The steepest reduction in the objective function occurs during the first 85 design iterations and after that the rate of reduction decreases gradually. These two points for switching from SPSA to BFGS and SA are considered: the switching point at the end of 800 design cycles of the SPSA method to see if the hybrid optimization method can further reduce the objective function and that after 85 design cycles of the SPSA method to see if design computational cost of the optimal solutions can be reduced significantly. From Fig. 1b, it can be seen that, for the SA method, after 1200 accepted function evaluations, the slope turns flat; therefore, the switch point is selected at 1200 accepted function evaluations of the SA method.

Figures 3 and 4 show the design results obtained by the hybrid SPSA method with different switch points. Figures 3a and 3b compare the convergence histories of the objective functions with design cycles and function evaluations of SPSA, SPSA+BFGS, and SPSA+SA methods for the two cases of hybrid SPSA (i.e., the switchover is activated at the end of 800 and 85 design cycles of the SPSA method, respectively). From Fig. 3a, it can be seen that the SPSA+BFGS method appears to have a higher local convergence rate than that of the SPSA and SPSA+SA methods. The final objective function value reached by SPSA+BFGS and SPSA+SA methods are 0.003369 and 0.003427, respectively. These values are of the same order and much smaller than the value of 0.012 reached by the SPSA method. The computational cost of SPSA+BFGS is also significantly cheaper than that of SPSA or SPSA+SA because it involves only 271 function evaluations compared to the 800 design cycles of SPSA. From Fig. 3b, it can be seen that SPSA+BFGS method reduced the objective function value of 0.0028 in 402 function evaluations of BFGS after 85 design cycles of SPSA, whereas the hybrid of SPSA and SA methods requires 2521 function evaluations of the SA method besides the 85 design cycles of the SPSA method to reduce the objective function value to 0.0031, which is more expensive than that of the SPSA+BFGS method. The convergence of the hybrid SA method is shown in Fig. 1b. It can be seen that the SA+BFGS method reduced the objective function value to 0.0027 in 472 function evaluations of BFGS besides the 1200 accepted function evaluations for the SA method.

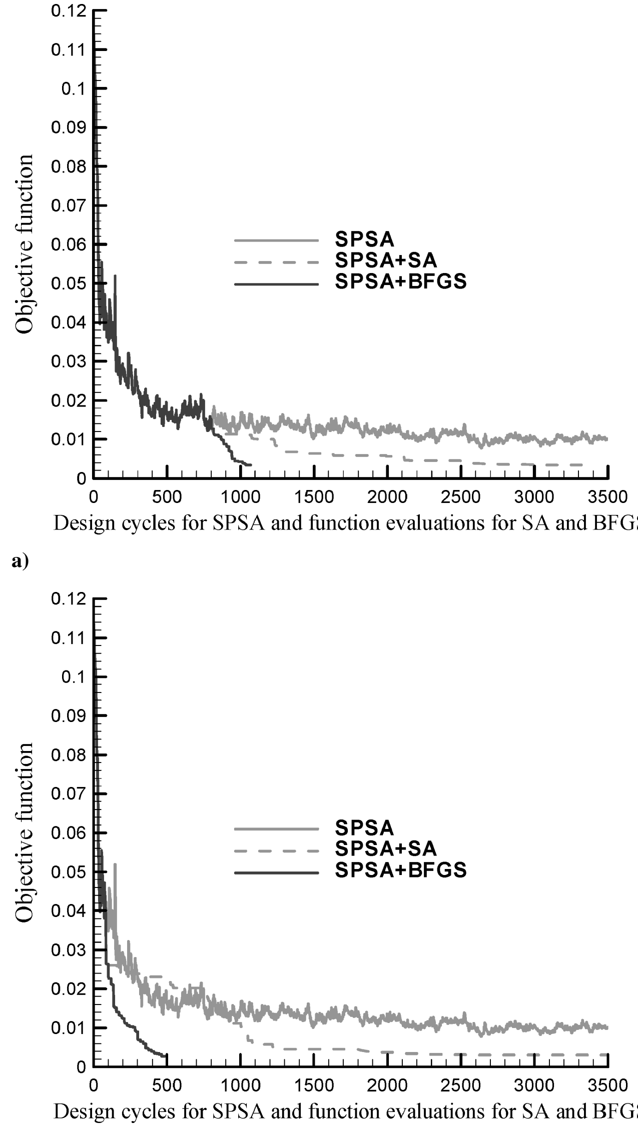

Fig. 3 Comparison of the convergence histories of the inverse design problem obtained by the SPSA method and hybrid methods with switchover points at a) 800 design cycles of the SPSA method and b) 85 design cycles of the SPSA method.

Figure 4a compares the initial, the target, and the final designed airfoil shapes and Fig. 4b compares the corresponding airfoil surface pressure coefficient distributions of the initial, target, and final designed airfoils obtained by SPSA+SA and SPSA+BFGS methods. It can be seen that the airfoil shapes and the surface pressure coefficients obtained by the hybrid methods are in good agreement with that of the target airfoil. Figure 4c compares the initial, the target, and the final designed airfoil shapes, and Fig. 4d compares the corresponding airfoil surface pressure coefficient distributions of the initial, target, and final designed airfoils obtained by the hybrid SA method. The airfoil shapes and the surface pressure coefficients obtained by the hybrid SA are also in good agreement with that of the target airfoil. The hybrid optimization methods, especially the hybrid stochastic methods with the BFGS method, not only obviously improved the design accuracy, but they also reduced the computational cost significantly, provided the switchover point was chosen properly. Details of switchover point selection and its impact on the solutions have been addressed by Xing and Damodaran.[42]

Figure 5 shows the evolution of the airfoil shape and the computational grid from the initial NACA 0012 airfoil to the target RAE 2822 airfoil during the design process. The evolution of the grid

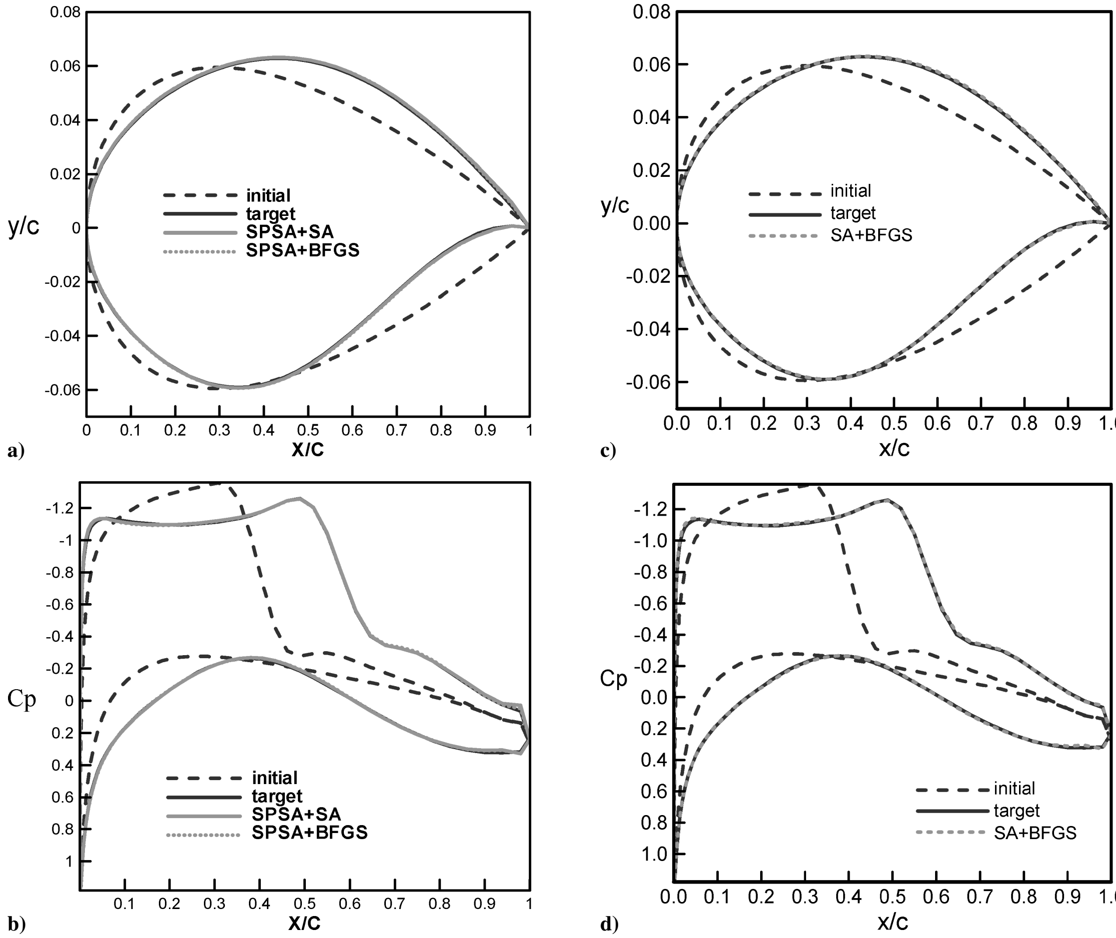

Fig. 4 Comparison of the initial, target, and designed results of a) airfoil shapes and b) airfoil surface pressure coefficient distributions: obtained by hybrid SPSA with switchover point at 85 design cycles and c) airfoil shapes and d) airfoil surface pressure distributions by hybrid SA.

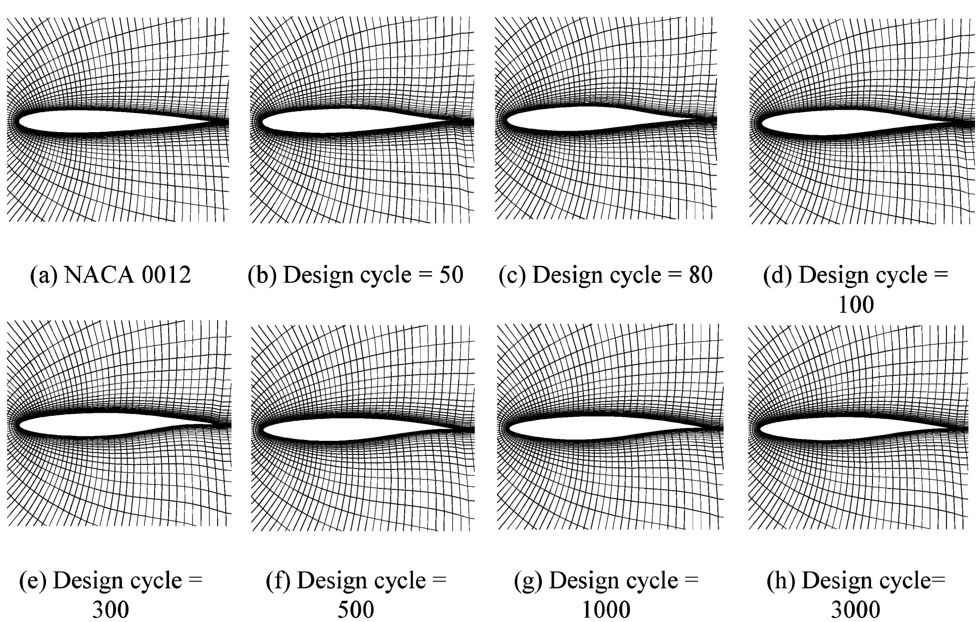

Fig. 5 Evolution of the computational grid and airfoil shape during the inverse design process.

shows the adjustment of the entire computational grid based on the perturbations imposed on the airfoil profile. The effect of values of random number and the tuning parameters pertaining to the SPSA method on the convergence process of the SPSA method are also investigated. Figure 6 shows the convergence histories of the inverse design problem with different random seeds. It can be seen that the convergence processes are not same, but the convergence speed and the final objective function values are very similar. Choice of the coefficients and parameters pertaining to the algorithm is critical to the performance of the SPSA, as is the case with all other stochastic methods such as SA, and useful guidelines for choosing the values of these coefficients and parameters are outlined by Spall,[15−17] Fabian,[26] Chin,[28] and Dippon and Renz.[29] As long as the parameters are selected properly according to the guidelines, they will not affect the convergence speed and final design results very much.

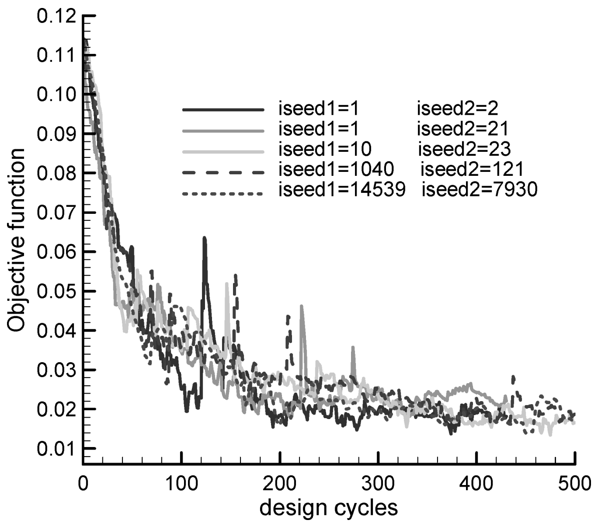

Fig. 6 Effect of random number seeds on the convergence of the SPSA method for inverse airfoil design problem.

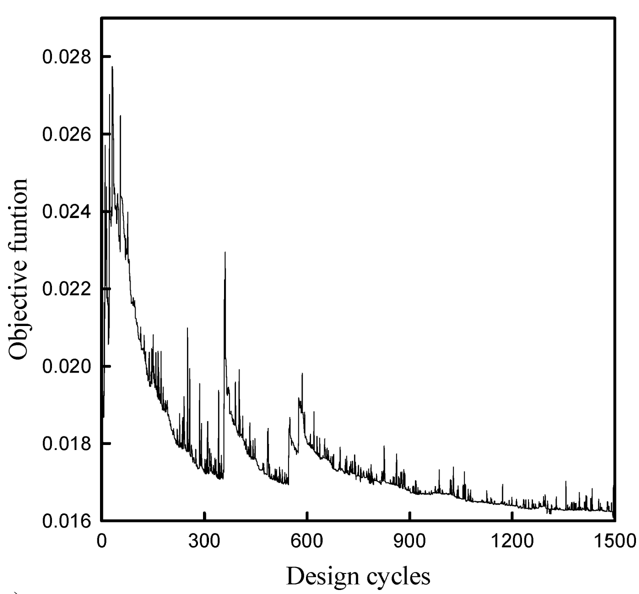

a)

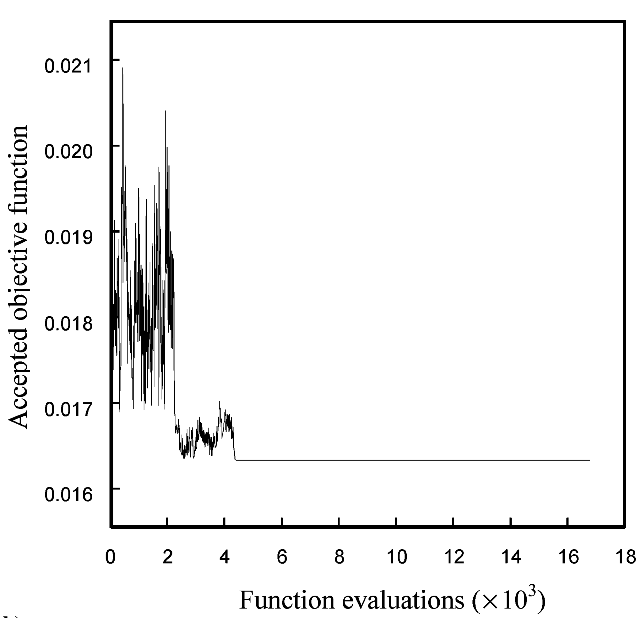

b)

Fig. 7 Convergence history of the constrained problem: a) SPSA and b) SA methods.

Transonic Airfoil Drag Minimization

Figure 7a shows the computed convergence history of the objective function obtained by the SPSA method for the transonic airfoil drag minimization problem. The computed results show that the airfoil shape obtained from the SPSA method yields a reduction in the coefficient of drag C_d by 9.78% (from 0.01800 to 0.01624) and both C_l and the airfoil section area satisfy the constraints defined by Eq. (6). The computed results agree well with the results obtained by Lee and Damodaran[31,33] using the SA method. However, the computational costs are very different. In this study, it can be seen that the SPSA method requires about 1489 iterations or 4467 function evaluations to reach convergence, whereas the SA method requires about 4500 accepted objective function evaluations (or a total of 9000 function evaluations) resulting in a reduction of 11.1% (from 0.01800 to 0.0160) in the coefficient of drag, C_d, as shown in Fig. 7b. Hence, the SPSA method results in an obvious gain in efficiency in terms of computational cost for this optimization problem. The computed airfoil shapes and surface pressure coefficient distributions of the baseline airfoil and the final designed airfoils are compared in Fig. 8. Figure 8a compares the initial airfoil shape and the designed shape obtained by using SPSA, whereas Fig. 8b compares the initial shape and the designed airfoil shape obtained by using the SA method. By comparing the baseline airfoil with the final designed airfoil shape obtained using SPSA, as shown in Fig. 8a, it can be seen that the main modification on the suction surface of the airfoil appears in the region that lies between the normalized chordwise position $x/c = 0.5$ and 0.8, whereas the modification on the pressure surface appears in the region located from $x/c = 0.25$ to 0.65. From the airfoil shape before and after optimization by SA the method, as shown in Fig. 8b, it can be seen that the modification on the suction surface and pressure surface is distributed evenly over the entire airfoil profile. However, the final shapes obtained by the SPSA and SA methods are similar and, when compared with the baseline airfoil, the thickness of the final designed airfoils appears to have increased in the region between $x/c = 0.5$ and 0.8 and appears to have marginally decreased or remained unchanged before $x/c = 0.5$.

Figure 8c compares the initial and designed airfoil surface pressure coefficient distributions obtained by the SPSA method, whereas Fig. 8d compares the initial and designed airfoil surface pressure coefficient distributions obtained by the SA method. Figure 8c also compares the computed surface pressure distributions with the experimental data from Cook et al.[40] (case 9) for the RAE 2822 airfoil at a Mach number of 0.726, angle of attack of $\alpha = 2.44$ deg, and Reynolds number of $Re = 6.5 \times 10^6$. The good agreement between the computed and experimental data suggests that the numerical simulation is reasonably accurate. It can be seen that the final pressure distributions on the suction surface obtained by SPSA and SA methods are totally different from that of the baseline. Before optimization, a strong shock wave can be seen to be located between $x/c = 0.5$ and 0.65, whereas the shock wave appears to be weakened considerably after constrained optimization using SPSA and SA. Figures 9a and 9b show the computed contours of local Mach number of the baseline airfoil and the designed airfoil using the SPSA method. From the Mach-number contours, it can be seen that the shock wave has been weakened considerably, resulting in a lower drag coefficient.

Axisymmetric Nozzle Shape Design Optimization

The aim of the design optimization is to determine the inlet expansion half-angle α_1 and outlet expansion half-angle α_2 to determine the optimal shape of the nozzle that maximizes the thrust of the nozzle. Figures 10a and 10b compare the convergence histories obtained by SPSA and SA methods, respectively. It can be seen that the SPSA method requires 4 iterations (i.e., 12 function evaluations) to get a value very close to the converged result, whereas the SA method requires 15 accepted (or 30 total) function evaluations to get a value close to the converged result. The computational cost of the SPSA method is only 50% of the cost of the SA method with the same converged objective function values. Figure 11a shows the computed local pressure contours of the original nozzle shape, which is the

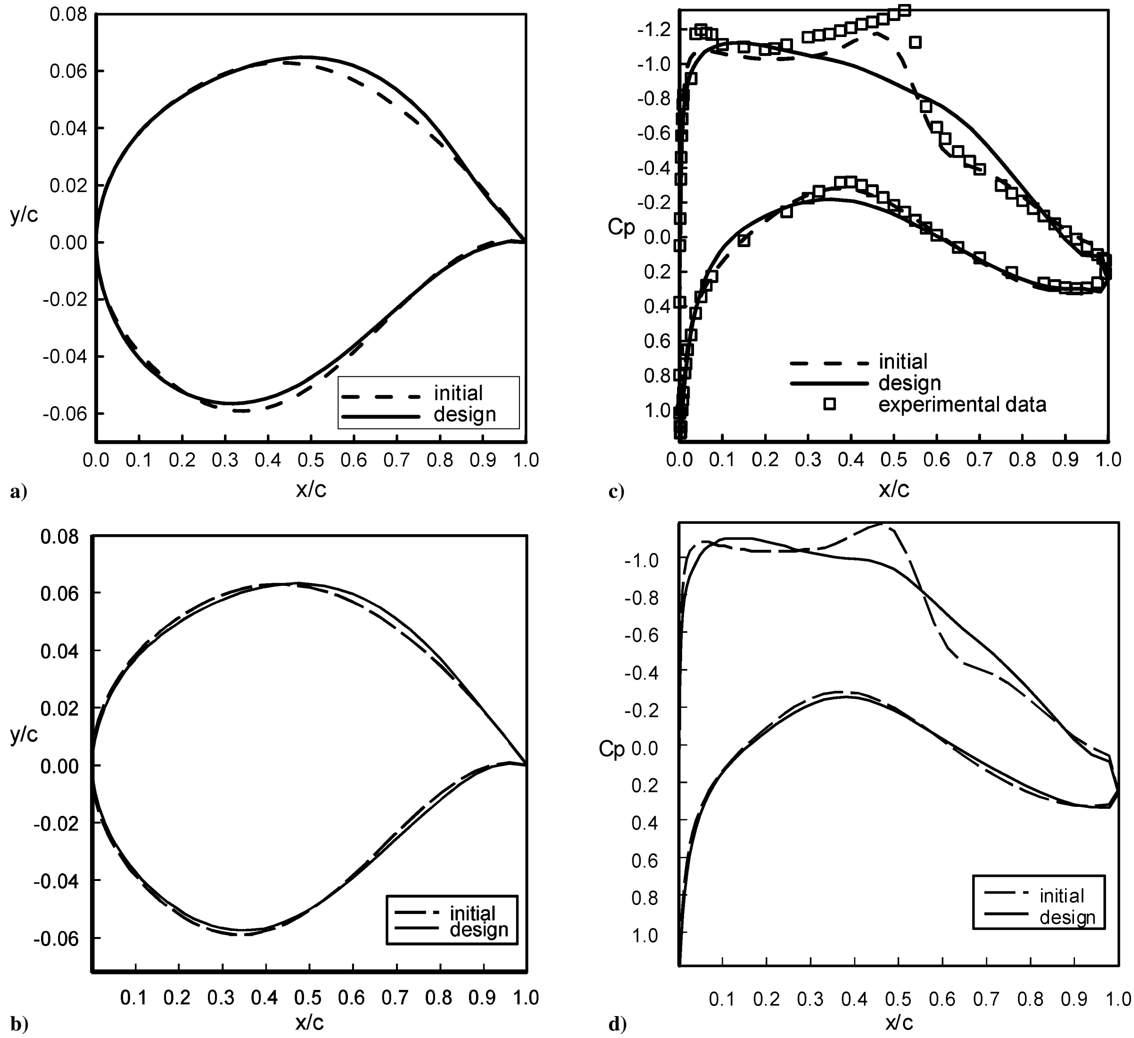

Fig. 8 Initial and designed airfoil shapes obtained by a) SPSA and b) SA methods and surface pressure coefficient distributions obtained by c) SPSA and d) SA method.

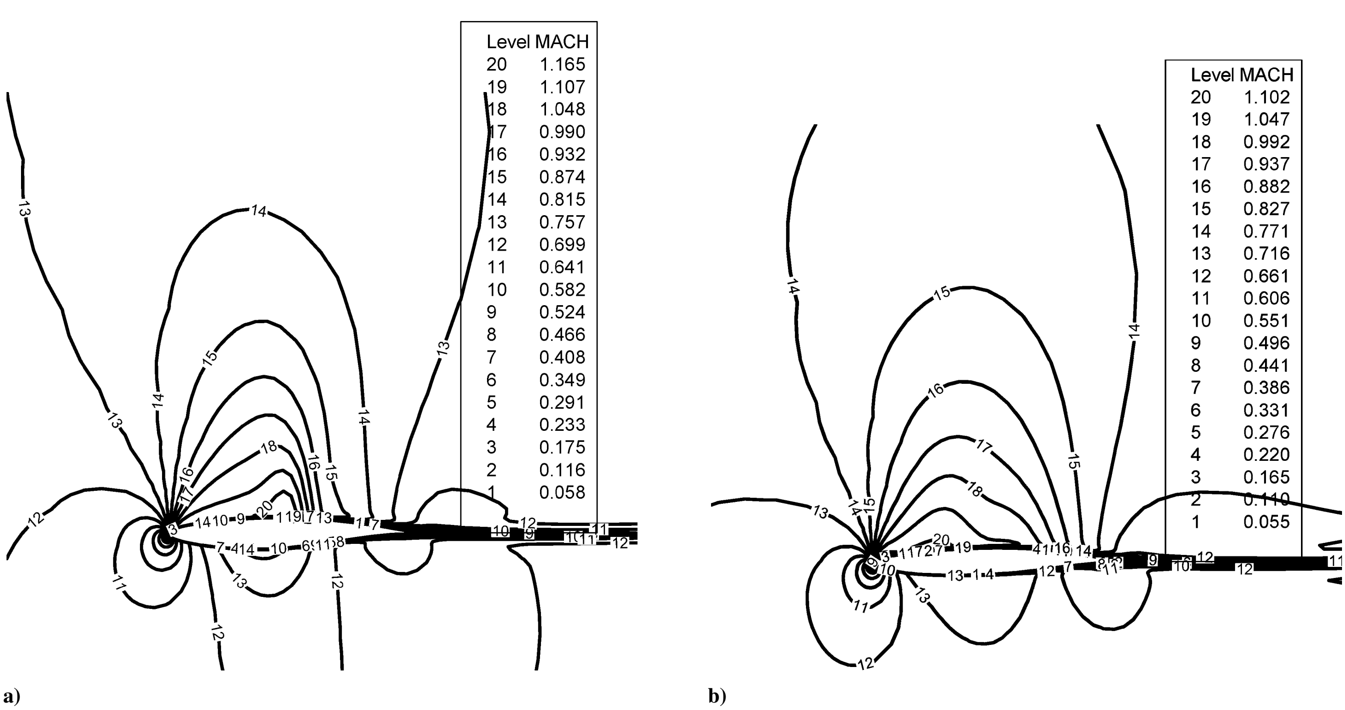

Fig. 9 Mach-number contours of the a) baseline airfoil and b) final designed airfoil.

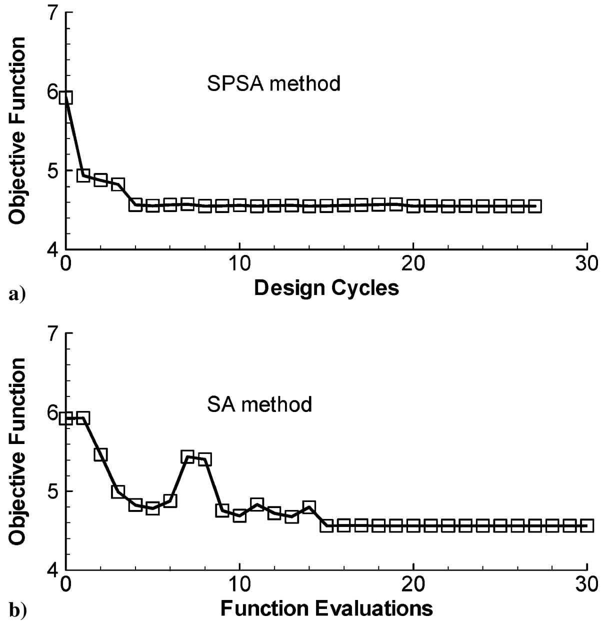

Fig. 10 Comparison of convergence histories of the nozzle shape design problem using SPSA and SA methods.

baseline flowfield for the optimization studies. Figure 11b shows the computed flowfield of the optimized nozzle shape. The comparison of Fig. 11a with Fig. 11b shows that the nozzle shape has changed to a certain extent from the original shape and the reduction of the pressure from the inlet to exit of the optimized nozzle is more than that corresponding to the baseline nozzle. Consequently, it has a higher thrust on the whole nozzle. Figure 12 shows the effect of the SPSA tuning parameter A $[a_k = a_0/(A+k)^\alpha]$ on the convergence of the optimization process for the two-dimensional nozzle shape design problem. It can be seen that the convergence speed and the final design results are independent of the value of the parameter A as long as A is selected according to the guidelines specified by Spall,[15–17] Fabian,[26] Chin,[28] and Dippon and Renz.[29]

Influence of Grid Size on the Values of Objective Functions

For the aforementioned test cases, the sensitivity of the converged values of the objective functions on the size of the computational mesh is demonstrated by carrying out the optimization using the same SPSA tuning parameters but using meshes of different grid sizes. For the airfoil inverse design and drag minimization problem, the grid size dependence studies have been done on 64×24, 128×48, and 256×96 meshes and satisfy the same convergence criteria for objective function convergence. Figures 13a and 13b show the influence of grid size on the objective function values attained by the method of tracking a parameter, which is defined as the decrease in the value of the objective function value; that is, $(F_0 - F)/F_0$ for the inverse airfoil design problem and drag minimization problem, where F_0 and F are, respectively, the initial value of the objective function and the final optimal value of the objective function obtained on the different meshes. It can be seen that the finer the grid, the lesser the reduction in the value of the objective function. The reduction in the value of the objective function for each design problem converges to an asymptotic limit as the grid size is increased. For the nozzle design problem, a grid size dependence study has been done on meshes with 31×81, 41×101, and 41×131 grid points. The convergence criteria used is the same for all the meshes. The variation of the value of $(f_0 - f)/f_0$ based on the objective function value at the end of the design optimization on different grids is shown in Fig. 13c. It can be seen that, as the grid is refined, the parameter shows a tendency to converge to some limiting value. From Fig. 13, it can be seen that the change in the value of the objective function corresponding to each design problem demonstrates a general tendency to converge to a limiting value as the grid is refined. For the inverse design problem and transonic

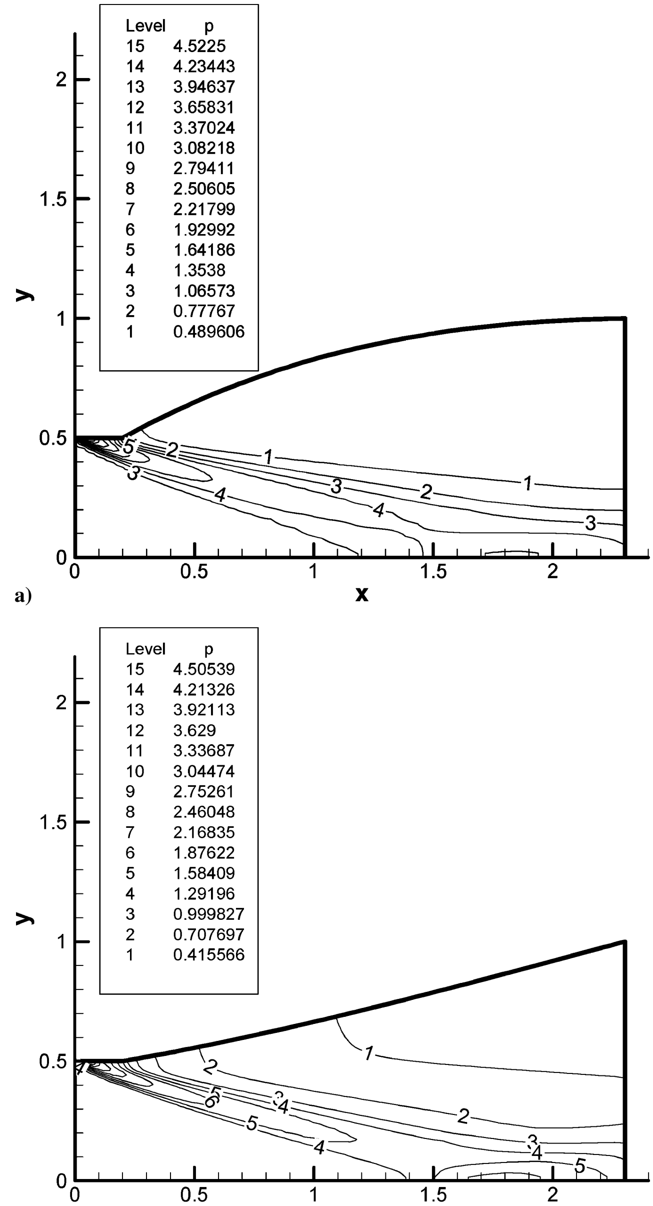

Fig. 11 Flowfields and shapes of the a) baseline nozzle and b) final designed nozzle.

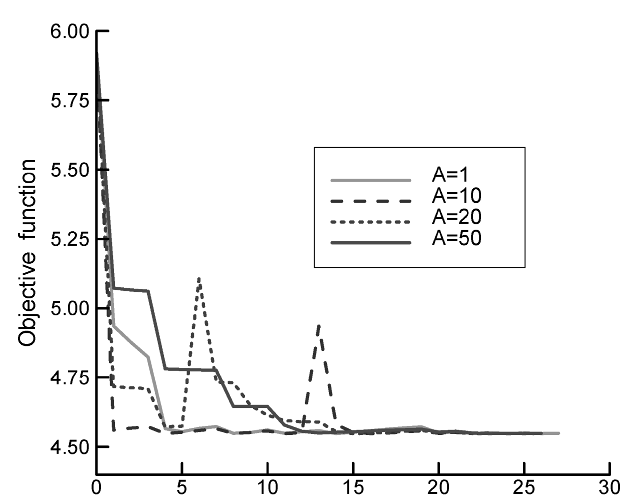

Fig. 12 Effect of SPSA tuning parameter A on the convergence of the optimization method for the nozzle shape design optimization problem.

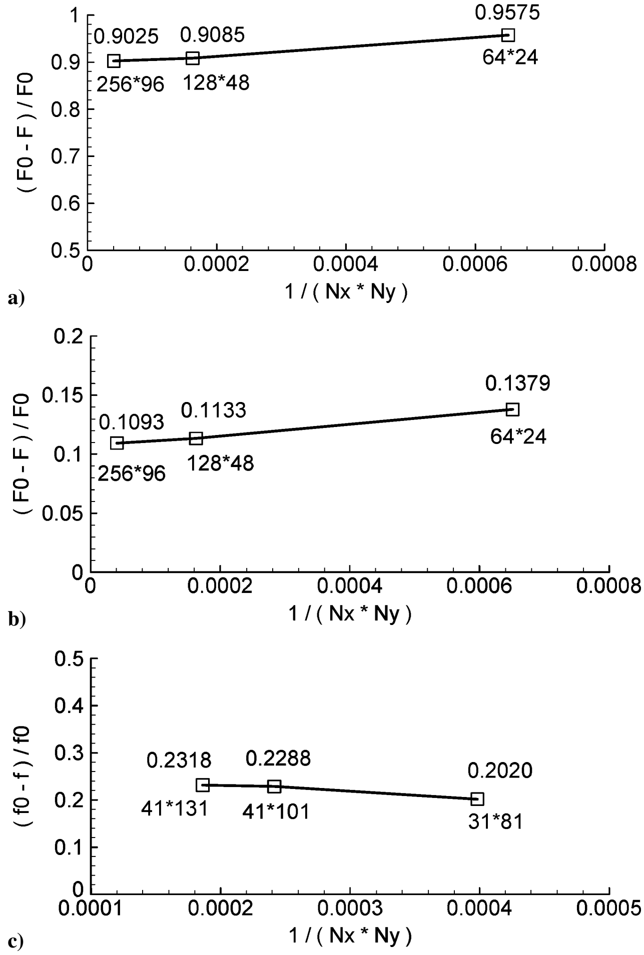

Fig. 13 Influence of grid size on the objective function values of a) airfoil inverse shape design problem, b) transonic airfoil drag minimization problem, and c) axisymmetric nozzle design problem.

drag minimization problem, as the grid is refined from 128×48 to 256×96, the change in the objective function value is smaller than that which occurred when the grid was coarsened from 128×48 to 64×24. Hence, a grid size of 128×48 used for airfoil problems in this study should be good enough to produce a fairly good economical estimate. Similarly, a 41×101 grid-point mesh used for the nozzle design problem can also produce a fairly good estimate for the nozzle shape design problem. The effect of using optimal solutions obtained on intermediate grids to analyze optimal solutions on finer grids on the performance of the optimization process will be addressed in a separate study in due course.

Conclusions

The SPSA method has been successfully implemented for aerodynamic shape design optimization problems, including inverse and constrained airfoil design and axisymmetric nozzle design, in this study. Results show that SPSA is able to find the optima of the design optimization problems considered in this paper and that the optimization algorithm can be easily implemented and integrated with the CFD code. Compared with SA algorithm, SPSA is able to decrease the computational costs significantly. For the problem of inverse airfoil design, the satisfaction of the termination criteria by the SPSA method appears to show that SPSA tends to be slightly less accurate than the SA method. SPSA results in an objective function value reaching a converged value by oscillating slightly about some mean value. This can be improved by combining the SPSA method with other optimization methods, such as a local search method, when the objective function reaches a point where it starts to oscillate about the converged value. Thus, the global optimum zone can be found by the SPSA method quickly while the accuracy can be improved by the local optimal methods by taking advantage of the rapid global search capability of the SPSA method and high accuracy of other methods simultaneously. The SPSA method shows higher convergence speed compared with the SA method for the drag minimization problem and the nozzle shape design problem, with almost the same optimization benefits as that of the SA method. From the results, it can be concluded that the SPSA method is a feasible optimization method that can be used to handle complex design problems. It is also relatively easy to implement. SPSA requires only two measurements of the objective function to approximate the gradient regardless of the dimensions of the design space corresponding to the optimization problem and, consequently, the cost of optimization decreases compared with global optimizers such as SA.

References

[1]Sobieszcaanski-Sobieski, J., and Haftka, R. T., "Multidisciplinary Aerospace Design Optimization: Survey of Recent Developments," AIAA Paper 96-0711, Jan. 1996.

[2]Aly, S., Ogot, M. M., and Pelz, R., "Stochastic Approach to Optimal Aerodynamic Shape Design," *Journal of Aircraft*, Vol. 33, No. 5, 1996, pp. 956–961.

[3]Quagliarella, D., and Cioppa, A. D., "Genetic Algorithms Applied to the Aerodynamic Design of Transonic Airfoils," AIAA Paper 94-1896, June 1994.

[4]Yamamoto, K., and Inoue, O., "Applications of Genetic Algorithm to Aerodynamic Shape Optimization," *12th AIAA Computational Fluid Dynamics Conference*, CP956, AIAA, Washington, DC, 1995, pp. 43–51.

[5]Cao, H. V., and Blom, G. A., "Navier–Stokes/Genetic Optimization of Multi-Element Airfoils," AIAA Paper 96-2487, June 1996.

[6]Benini, E., and Tourlidakis, A., "Design Optimization of Vaned Diffusers for Centrifugal Compressors Using Genetic Algorithms," AIAA Paper 2001-2583, June 2001.

[7]Gallego, R. A., Alves, A. B., Monticelli, A. A., and Romero, R., "Parallel Simulated Annealing Applied to Long Term Transmission Network Expansion Planning," *IEEE Transactions on Power Systems*, Vol. 12, No. 1, 1997, pp. 181–189.

[8]Bhandarkar, S. M., and Machaka, S., "Chromosome Reconstruction from Physical Maps Using a Cluster of Workstations," *Journal of Supercomputing*, Vol. 11, No. 1, 1997, pp. 61–87.

[9]Aarts, E., and Korst, J., *Simulated Annealing and Boltzmann Machines, A Stochastic Approach to Combinatorial Optimization and Neural Computing*, Wiley, New York, 1989, p. 12.

[10]Diekmann, R., Luling, R., and Simon, J., "Problem Independent Distribution Simulated Annealing and Its Applications," *Applied Simulated Annealing*, Lecture Notes in Economics and Mathematical Systems, Vol. 396, Springer-Verlag, New York, 1993, pp. 17–44.

[11]Wang, X., and Damodaran, M., "Comparison of Deterministic and Stochastic Optimization Algorithms for Generic Wing Design Problems," *Journal of Aircraft*, Vol. 37, No. 5, 2000, pp. 929–932.

[12]Wang, X., and Damodaran, M., "Aerodynamic Shape Optimization Using Computational Fluid Dynamics and Parallel Simulated Annealing Algorithms," *AIAA Journal*, Vol. 38, No. 8, 2001, pp. 1500–1508.

[13]Vicini, A., and Quagliarella, D., "A Multi-Objective Approach to Transonic Wing Design by Means of Genetic Algorithms," *NATO RTO/AVT Symposium on Aerodynamic Design and Optimization*, Ottawa, 1999.

[14]Hämäläinen, J. P., Mäkinen, R. A. E., Tarvainen, P., and Toivanen, J., "Evolutionary Shape Optimization in CFD with Industrial Applications," *Proceedings of ECCOMAS 2000 Conference*, European Congress on Computational Methods in Applied Sciences and Engineering, Barcelona, 2000.

[15]Spall, J. C., "Multivariate Stochastic Approximation Using a Simultaneous Perturbation Gradient Approximation," *IEEE Transactions on Automatic Control*, Vol. 37, No. 3, 1992, pp. 332–341.

[16]Spall, J. C., "An Overview of the Simultaneous Perturbation Method for Efficient Optimization," *Johns Hopkins APL Technical Digest*, Vol. 19, No. 4, 1998, pp. 482–492.

[17]Spall, J. C., "Implementation of the Simultaneous Perturbation Algorithm for Stochastic Optimization," *IEEE Transactions on Aerospace and Electronic Systems*, Vol. 34, No. 3, 1998, pp. 817–823.

[18]Alessandri, A., and Parisini, T., "Nonlinear Modelling of Complex Large-Scale Plants Using Neural Networks and Stochastic Approximation," *IEEE Transactions on Systems, Man, and Cybernetics—A*, Vol. 27, No. 6, 1997, pp. 750–757.

[19]Bhatnagar, S., Fu, M. C., Marcus, S. I., and Fard, P. J., "Optimal Structured Feedback Policies for ABR Flow Control Using Two Timescale SPSA," *IEEE/ACM Transactions on Networking*, Vol. 9, No. 4, 2001, pp. 479–491.

[20]Chin, D. C., and Smith, R. H., "A Traffic Simulation for Mid-Manhattan with Model-Free Adaptive Signal Control," *Proceedings of the Summer Computer Simulation Conference*, Society for Computer Simulation, San Diego, CA, 1994, pp. 296–301.

[21]Koch, M. I., Chin, D. C., and Smith, R. H., "Network-Wide Approach to Optimal Signal Light Timing for Integrated Transit Vehicle and Traffic Operations," *Proceedings of the 7th National Conference on Light Rail Transit*, Vol. 2, National Academy of Sciences Press, Washington, DC, 1997, pp. 126–131.

[22]Bhatnagar, S., Fu, M. C., Marcus, S. I., and Bhatnagar, S., "Two Timescale Algorithms for Simulation Optimization of Hidden Markov Models," *IIE Transactions*, Vol. 33, No. 3, 2001, pp. 245–258.

[23]Maeda, Y., and Tsushio, K., "Blind Signal Separation via Simultaneous Perturbation Method," *Proceedings of the International Joint Conference on Neural Networks*, IEEE World Congress on Computational Intelligence, Honolulu, HI, 2002.

[24]Tayong, H., Beasley, A., Cole-Rhodes, A., and Cooper, A. B., "Adaptive Optimization of a Parametric Receiver for Fast Frequency-Hopping," 36th Annual Conf. on Information Sciences and Systems, Princeton, NJ, Paper 180, March 2002.

[25]Xing, X. Q., and Damodaran, M., "Assessment of the Simultaneous Perturbation Stochastic Approximation Method for Wing Design Optimization Problem," *Journal of Aircraft*, Vol. 39, No. 2, 2002, pp. 379–381.

[26]Fabian, V., "Stochastic Approximation," *Optimizing Methods in Statistics*, edited by J. J. Rustigi, Academic Press, New York, 1971, pp. 439–470.

[27]Kushner, H. J., and Yin, G. G., *Stochastic Approximation Algorithms and Applications*, Springer-Verlag, New York, 1997.

[28]Chin, D. C., "Comparative Study of Stochastic Algorithms for System Optimization Based on Gradient Approximations," *IEEE Transactions on Systems, Man, and Cybernetics*, Vol. 27, No. 2, 1997, pp. 244–249.

[29]Dippon, J., and Renz, J., "Weighted Means in Stochastic Approximation of Minima," *SIAM Journal on Control and Optimization*, Vol. 35, No. 5, 1997, pp. 1811–1827.

[30]Deb, K., *Optimization for Engineering Design, Algorithms and Examples*, Prentice-Hall, New Delhi, India, 1998.

[31]Lee, S. L., "Aerodynamic Shape Design of Transonic Airfoils Using Stochastic Optimization Methods and Computational Fluid Dynamics," Ph.D. Dissertation, School of Mechanical and Production Engineering, Nanyang Technological Univ., Singapore, Sept. 1999.

[32]Hicks, R. M., and Henne, P. A., "Wing Design by Numerical Optimization," AIAA Paper 79-0080, Jan. 1979.

[33]Lee, S. L., and Damodaran, M., "Aerodynamic Design of Transonic Airfoils Using Simulated Annealing and Navier–Stokes Equations," AIAA Paper 2000-0782, Jan. 2000.

[34]Jameson, A., Schmidt, W., and Turkel, E., "Numerical Solutions of the Euler Equations by Finite-Volume Methods Using Runge–Kutta Time Stepping Schemes," AIAA Paper 81-1259, June 1981.

[35]Martinelli, L., Jameson, A., and Grasso, F., "A Multi-Grid Method for Navier–Stokes Equations," AIAA Paper 86-0208, Jan. 1986.

[36]Damodaran, M., and Lee, K. H., "Finite Volume Calculation of Steady Viscous Compressible Flow past Airfoils," *Journal of the Institution of Engineers*, Vol. 33, No. 5, 1993, pp. 39–44.

[37]Yoon, S., and Jameson, A., "Lower–Upper Symmetric-Gauss–Seidal Method for the Euler and Navier–Stokes Equations," *AIAA Journal*, Vol. 26, No. 9, 1988, pp. 1025, 1026.

[38]Yee, H. C., and Harten, A., "Implicit TVD Schemes for Hyperbolic Conservation Laws in Curvilinear Coordinates," *AIAA Journal*, Vol. 25, No. 2, 1987, pp. 266–274.

[39]Wang, X., Spiegler, E., and Timnat, Y. M., "Optimization of Ram Accelerators System Design," *Journal of Propulsion and Power*, Vol. 16, No. 2, 2000, pp. 269–277.

[40]Cook, P. H., McDonald, M. A., and Firmin, M. C. P., "Aerofoil RAE2822—Pressure Distributions, and Boundary Layer and Wake Measurement," AGARD-AR-138, Paper A6, 1979.

[41]Press, W. H., Flannery, B. P., Teukolsky, S. A., and Vetterling, W. T., *Numerical Recipes in C, The Art of Scientific Computing*, Cambridge Univ. Press, Cambridge, England, U.K., 1988.

[42]Xing, X. Q., and Damodaran, M., "Aerodynamic Shape Design Optimization Using Hybrid Stochastic and Deterministic Optimization Methods and CFD," AIAA Paper 2003-3786, June 2003.

A. Berman
Associate Editor